INSTITUTE OF PHYSICS PUBLISHING JOURNAL OF PHYSICS B: ATOMIC, MOLECULAR AND OPTICAL PHYSICS

J. Phys. B: At. Mol. Opt. Phys. **39** (2006) 455–462 doi:10.1088/0953-4075/39/2/019

Differential cross sections for electron impact excitation out of the (. . . 6s6p $^1P_1$) state of barium

P W Zetner and P V Johnson[1]

Department of Physics and Astronomy, University of Manitoba, Winnipeg, MB R3T 2N2, Canada

Received 8 September 2005
Published 19 December 2005
Online at stacks.iop.org/JPhysB/39/455

Abstract

Differential cross sections for electron impact on excited state barium atoms have been measured for 20 eV incident electron energy and scattering angles of 5.5°, 9°, 13° and 16°. Results for the excitations (. . . 6s6p $^1P_1$) → X are presented with X = (. . . 6s7s $^1S_0$), (. . . 6s7p $^1P_1$), (. . . 5d^2 $^1D_2$ + . . . 5d6p $^1D_2$), (. . . 5d^2 $^3P_2$) and (. . . 6s6d $^1D_2$). Comparisons are made with existing theoretical results calculated in the convergent close coupling formalism and the unitarized distorted wave approximation.

Introduction

There has been considerable progress in the theoretical description of electron scattering from rather complex atomic targets. The barium atom has been a focus of recent theoretical work because of a fairly extensive set of available experimental data and because of interest in this atom as a possible candidate for efficient (discharge) lighting [1, 2]. The convergent close coupling (CCC) method has been particularly successful in describing electron impact processes involving excited state barium atoms [2]. Electron impact coherence parameters (EICP) describing orientation and alignment of the (. . . 6s6p $^1P_1$) state in superelastic processes of the type X → (. . . 6s6p $^1P_1$), for higher lying levels, X, have been measured and are, generally, well described by this theoretical approach [3, 4].

In this paper, we report measured differential cross sections (DCS) for excitation of higher lying states out of the (. . . 6s6p $^1P_1$) state of barium. Some of these have recently been employed in the determination of integral cross sections for excitation out of the P state [2] but have, as yet, remained unpublished. We present the DCS for the excitations (. . . 6s6p $^1P_1$) → X for final levels X = (. . . 6s7s $^1S_0$), (. . . 6s7p $^1P_1$), (. . . 5d^2 $^1D_2$ + . . . 5d6p $^1D_2$), (. . . 5d^2 $^3P_2$) and (. . . 6s6d $^1D_2$) at 20 eV impact energy. Final level designations correspond to the dominant LS terms in the configuration–interaction (CI) expansions determined in the structure calculations associated with the CCC method [3]. For convenience, we employ the notation of Zetner *et al* [5] in which a labelling number is attached to the particular

[1] Present address: Jet Propulsion Laboratory, Mailstop 183-601, 4800 Oak Grove Drive, Pasadena, CA, USA.

electron energy loss spectral feature associated with the excitation $(\ldots 6s6p\,{}^1P) \rightarrow X$. For $X = (\ldots 6s7s\,{}^1S_0)$, $(\ldots 6s7p\,{}^1P_1)$, $(\ldots 5d^2\,{}^1D_2 + \ldots 5d6p\,{}^1D_2)$, $(\ldots 5d^2\,{}^3P_2)$ and $(\ldots 6s6d\,{}^1D_2)$, the corresponding feature numbers are 6, 7, 1, 3 and 8, respectively. Partial differential cross sections (PDCS) for two of these excitations, namely $X = (\ldots 5d^2\,{}^3P_2)$ and $(\ldots 6s6d\,{}^1D_2)$, have been reported earlier [5]. The PDCS differ from the DCS in that they describe excitation out of an aligned and/or oriented P level. The DCS describes excitation out of an isotropic P level. The connection between the PDCS and the DCS is discussed below. Our measured DCS are compared with available theoretical results calculated in the CCC formalism [3] and the unitarized distorted wave approximation (UDWA) described in Zetner *et al* [5].

Determination of the DCS

The apparatus consists of an electron spectrometer in which the electron source and scattered electron detector both employ single-hemisphere energy selection optics. Measurements were carried out with a system energy resolution of approximately 90 meV at about 75 nA electron gun current. The angular resolution of the spectrometer is estimated to be less than 5°. Magnetic-field compensation (to less than 25 mG) is accomplished by a single layer of 0.050 in. μ-metal shielding which is periodically degaussed.

The electron spectrometer is configured in such a way that the scattered electron detector is held fixed while the electron gun is rotatable. This established the most convenient geometry for our previous measurements of EICP associated with a 'time-reversed' process [4].

The metal vapour beam source consists of a tubular, 304 stainless-steel crucible wrapped with resistive, coaxial heating wire. It is heated to a typical operating temperature of 760 °C and produces a beam collimation of 10:1 with typical number densities of the order of 7×10^{10} cm^{-3} at the interaction region. During the measurement, background gas pressure in the chamber was typically less than 1×10^{-6} Torr.

Selection of the polarization state of the laser beam at the interaction region was accomplished by a phase retardation plate in tandem with a Glan–Taylor polarizing prism. The reader is referred to figure 1(a) of Johnson *et al* [6] for a schematic diagram of the apparatus. The collimated barium vapour beam is illuminated orthogonally by the laser beam tuned to the $(\ldots 6s^2\,{}^1S_0) \rightarrow (\ldots 6s6p\,{}^1P_1)$ resonance transition which produces a mixed target population of atoms in the ground $(\ldots 6s^2\,{}^1S_0)$, metastable $(\ldots 6s5d\,{}^1D_2,\ {}^3D_2)$ and short-lived $(\ldots 6s6p\,{}^1P_1)$ states. By a procedure described at length in [3], electron energy loss spectra containing only features arising from $(\ldots 6s6p\,{}^1P_1) \rightarrow X$ excitations can be produced. Feature intensities in these spectra depend on the relevant DCS as well as laser beam incidence direction and polarization state. To make this dependence explicit, we have defined [7] the PDCS which depend on the laser beam polarization state and polar angles (θ_v, ϕ_v) measured with respect to a quantization axis, taken in our work to be the (spatially fixed) scattered electron direction. For example, for linearly polarized laser light

$$\begin{aligned}\sigma^{\mathrm{PDCS}}(\Delta E;\theta_v,\phi_v,\psi) = \tfrac{3}{2}\sigma^{\mathrm{DCS}}(\Delta E)\big([1+\cos^2\theta_v - \sin^2\theta_v\cos 2\psi]\rho^c_{11} \\ + [\sin^2\theta_v(1+\cos 2\psi)]\rho^c_{00} - [(1+\cos^2\theta_v)\cos 2\phi_v\cos 2\psi \\ + 2\cos 2\phi_v \sin 2\psi - \sin^2\theta\cos 2\phi_v]\rho^c_{-11} \\ + \sqrt{2}[\sin 2\theta_v\cos\phi_v + \sin 2\theta_v\cos\phi_v\cos 2\psi \\ + 2\sin\theta_v\sin\phi_v\sin 2\psi]\,\mathrm{Re}\big[\rho^c_{01}\big]\big) \qquad (1)\end{aligned}$$

where $\sigma^{\mathrm{PDCS}}(\Delta E;\ \theta_v,\ \phi_v,\ \psi)$ is the partial differential cross section and $\sigma^{\mathrm{DCS}}(\Delta E)$ is the differential cross section for collisional process with excitation energy ΔE. The polarization

angle ψ of the linearly polarized light is measured with respect to the quantization axis. The quantities ρ^{c}_{ij} are collision frame density matrix elements for the P state produced in the 'time-inverse' electron collision [7]. Comparison of equation (1) with equation (3) of Li and Zetner [7] reveals differences in two terms where a factor of 2 was erroneously omitted in that work. We have used the laser geometry: $(\theta_v, \phi_v) = (90^\circ, 90^\circ)$ in which the laser beam is propagating vertically upwards striking the horizontal scattering plane from below. For this case, the PDCS becomes

$$\sigma^{\mathrm{PDCS}}(\Delta E; 90^\circ, 90^\circ, \psi) = \tfrac{3}{4}\sigma^{\mathrm{DCS}}(\Delta E)\big(1 - \cos 2\psi + (1 + 3\cos 2\psi)\rho^{c}_{00} - 2(1 - \cos 2\psi)\rho^{c}_{-11} + 4\sqrt{2}\sin 2\psi\ \mathrm{Re}\big[\rho^{c}_{01}\big]\big). \tag{2}$$

For circularly polarized laser light, using RHC (LHC) to designate right- (left-) hand circularly polarized light we have, in the $(\theta_v, \phi_v) = (90^\circ, 90^\circ)$ geometry,

$$\sigma^{\mathrm{PDCS}}(\Delta E; 90^\circ, 90^\circ, \mathrm{RHC}) = \tfrac{3}{4}\sigma^{\mathrm{DCS}}(\Delta E)\big(1 + \rho^{c}_{00} - 2\rho^{c}_{-11} + 4\sqrt{2}\,\mathrm{Im}\big[\rho^{c}_{01}\big]\big) \tag{3a}$$

$$\sigma^{\mathrm{PDCS}}(\Delta E; 90^\circ, 90^\circ, \mathrm{LHC}) = \tfrac{3}{4}\sigma^{\mathrm{DCS}}(\Delta E)\big(1 + \rho^{c}_{00} - 2\rho^{c}_{-11} - 4\sqrt{2}\,\mathrm{Im}\big[\rho^{c}_{01}\big]\big). \tag{3b}$$

Spectral feature intensity in an energy loss spectrum is directly proportional to the PDCS

$$I_P(\Delta E; \theta_v, \phi_v, \pi) \propto \sigma^{\mathrm{PDCS}}(\Delta E; \theta_v, \phi_v, \pi) \tag{4}$$

where I_P is the feature intensity, ΔE is the energy loss associated with a particular feature and π represents the polarization state of the laser beam.

It can readily be shown that for the $(\theta_v, \phi_v) = (90^\circ, 90^\circ)$ geometry the following relation holds:

$$\tfrac{1}{2}\{\sigma^{\mathrm{PDCS}}(\Delta E; 90^\circ, 90^\circ, \pi) + \sigma^{\mathrm{PDCS}}(\Delta E; 90^\circ, 90^\circ, \bar{\pi})\} = \tfrac{3}{2}(1 - h)\sigma^{\mathrm{DCS}}(\Delta E) \tag{5}$$

where π and $\bar{\pi}$ represent orthogonal polarization states (circular or linear) of the laser beam and h is the so-called 'height parameter' for the time-inverse collision process (terminating on the $(\ldots 6s6p\ ^1P_1)$ state). Equation (5) shows that, in the $(\theta_v, \phi_v) = (90^\circ, 90^\circ)$ geometry, the sum of electron energy loss feature intensities (for processes initiating on the P state) over orthogonal polarization states is proportional to the DCS multiplied by (1 − h). Our previous determinations of h [4] were used to extract the DCS. A normalization to the $(\ldots 6s^2\ ^1S_0) \rightarrow (\ldots 6s6p\ ^1P_1)$ DCS was used to place these DCS on an absolute scale utilizing the formula

$$\frac{I_P(\Delta E; 90^\circ, 90^\circ, \pi) + I_P(\Delta E; 90^\circ, 90^\circ, \bar{\pi})}{I_{SP}(\Delta E_{SP})} = \frac{3N_P(1 - h)\sigma^{\mathrm{DCS}}(\Delta E)}{N\sigma^{\mathrm{DCS}}_{SP}} \tag{6}$$

where $I_{SP}(\Delta E_{SP})$ is the electron energy loss spectral feature intensity for the $(\ldots 6s^2\ ^1S_0) \rightarrow (\ldots 6s6p\ ^1P_1)$ excitation (obtained with laser off), $\frac{N_P}{N}$ is the relative number of $(\ldots 6s6p\ ^1P_1)$ state scatterers in the target volume and $\sigma^{\mathrm{DCS}}_{SP}$ is the known DCS for the $(\ldots 6s^2\ ^1S_0) \rightarrow (\ldots 6s6p\ ^1P_1)$ excitation. We used the 20 eV measurements of Wang *et al* [8] for the normalizing cross sections, $\sigma^{\mathrm{DCS}}_{SP}$. Determination of the relative P state population, $\frac{N_P}{N}$, is discussed in [3].

Below we compare some of the present measurements with previous data [5]. Data reported in [5] refer to the PDCS determined with linearly polarized laser light and a geometry defined by $(\phi_v, \theta_v, \psi) = (45^\circ, 0^\circ, 54.7^\circ)$. For this geometry, the DCS is related to the

Table 1. Measured differential cross sections for the transitions $(\ldots 6s6p\ ^1P_1) \rightarrow$ X at 20 eV impact energy.

Final level, X	Initial level	Excitation energy (eV)	Differential cross section (10^{-16} cm^2 Sr^{-1}) 5.5°	9°	13°	16°
$(\ldots 5d^2\ ^1D_2) + (\ldots 5d6p\ ^1D_2)$	$(\ldots 6s6p\ ^1P_1)$	0.621	61.1 (18)	12.4 (4.6)	2.7 (1.2)	1.7 (0.9)
	$(\ldots 6s^2\ ^1S_0)$	2.860				
$(\ldots 5d^2\ ^3P_2)$	$(\ldots 6s6p\ ^1P_1)$	0.727	11.3 (3.4)	2.1 (0.8)	0.45 (0.2)	0.28 (0.14)
	$(\ldots 6s^2\ ^1S_0)$	2.966				
$(\ldots 6s7s\ ^1S_0)$	$(\ldots 6s6p\ ^1P_1)$	1.261	50.5 (15)	6.0 (2.2)	0.68 (0.3)	0.18 (0.09)
	$(\ldots 6s^2\ ^1S_0)$	3.500				
$(\ldots 6s7p\ ^1P_1)$	$(\ldots 6s6p\ ^1P_1)$	1.301	10.2 (3.1)	6.0 (2.2)	1.9 (0.85)	1.9 (0.98)
	$(\ldots 6s^2\ ^1S_0)$	3.540				
$(\ldots 6s6d\ ^1D_2)$	$(\ldots 6s6p\ ^1P_1)$	1.51	79.2 (24)	15.2 (5.6)	2.9 (1.3)	2.3 (1.2)
	$(\ldots 6s^2\ ^1S_0)$	3.749				

Table 2. Theoretical h parameter for superelastic transitions X $\rightarrow (\ldots 6s6p\ ^1P_1)$.

Final level, X	Impact energy (eV)	h Parameter 5.5°	9°	13°	16°
$(\ldots 5d^2\ ^1D_2) + (\ldots 5d6p\ ^1D_2)$	19.4	0.29	0.27	0.22	0.17
$(\ldots 5d^2\ ^3P_2)$	19.3	0.29	0.27	0.24	0.21
$(\ldots 6s7s\ ^1S_0)$	18.7	0	0	0	0
$(\ldots 6s7p\ ^1P_1)$	18.7	0.47	0.46	0.43	0.50
$(\ldots 6s6d\ ^1D_2)$	18.5	0.32	0.37	0.35	0.21

PDCS by

$$\sigma^{\mathrm{DCS}}(\Delta E) = \eta\sigma^{\mathrm{PDCS}}(\Delta E; 45^\circ, 0^\circ, 54.7^\circ) \tag{7}$$

where $\eta = 2[1+3h-(1-h)P_2]^{-1}$ and P_2 is a Stokes parameter for the time-inverse collision. Using previous determinations of P_2 and h [4], we extract the DCS from the PDCS for comparison with the present results.

Results

In table 1, we present the absolute DCS for 20 eV electron impact excitation of the transitions $(\ldots 6s6p\ ^1P_1) \rightarrow$ X for the indicated upper levels, X. In table 2, we show the h parameters used to convert the present PDCS into the DCS. These are theoretical h parameters calculated in the CCC formalism which agreed well with the measurements discussed in [4]. Likewise, in table 3, we show h and P_2 parameters required to effect the PDCS to DCS conversion in previous data [5] using equation (7). Figures 1–5 present the data graphically. The total uncertainty in the measured DCS arises from error contributions of the various terms in equation (6). Error limits on a specific P $\rightarrow$ X spectral feature intensity, I_{P}, were determined from the propagation of statistical uncertainties (in the various integrated feature intensities utilized) through the spectrum unfolding procedure described by Johnson *et al* [3]. Likewise, statistical uncertainties in I_{SP} and the relative P state population fraction, N_{P}/N, were determined. All statistical errors and the quoted uncertainty (25%) in the measured cross sections of Wang

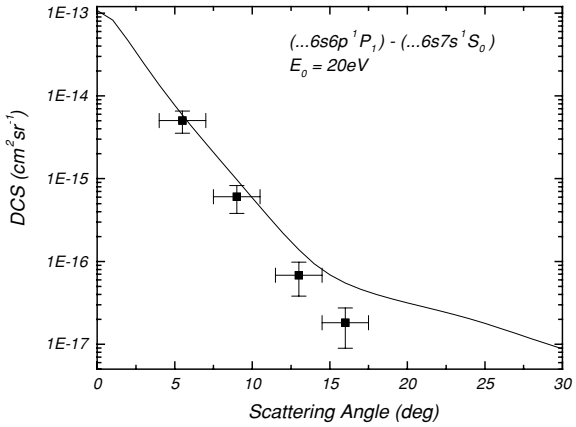

Figure 1. Differential cross sections for the $(\ldots 6s6p\ ^1P_1)$ to $(\ldots 6s7s\ ^1S_0)$ excitation at 20 eV. Solid squares with error bars represent the measured results. The solid curve shows the results of a CCC calculation [3].

Table 3. Theoretical Stokes and height parameters for superelastic transitions X → $(\ldots 6s6p\ ^1P_1)$ used in equation (7).

Final level, X	Impact energy (eV)	Scattering angle (°)	Stokes parameter, P_2 (CCC)	Height parameter, h (CCC)	η (equation (7))
$(\ldots 5d^2\ ^3P_2)$	19.3	5	0.016	0.32	1.03
		10	−0.24	0.38	0.87
		15	−0.43	0.26	0.95
		20	−0.42	0.13	1.14
$(\ldots 6s6d\ ^1D_2)$	18.5	5	0.032	0.29	1.08
		10	−0.0097	0.27	1.10
		15	−0.023	0.22	1.19
		20	−0.017	0.19	1.26

et al [8] were added in quadrature to give the total error. We did not include an error contribution from the (theoretical) h parameters employed in equation (6).

Generally, good agreement between CCC theory and experiment is shown in all cases. The theory shows strong forward-peaking characteristic of dipole-allowed transitions. This result is consistent with the presence of LS terms in the configuration–interaction (CI) expansions of the initial and final state CCC wavefunctions which allow dipole coupling. In the kinematic regime studied here (20 eV impact energy and small scattering angles), the excitation is characterized by low momentum transfer and will be dominated by these dipole-coupled terms. Dominant LS terms and mixing coefficients in the CI expansions are listed in table 1 of Johnson *et al* [3]. For final states X = $(\ldots 6s7s\ ^1S_0)$ and $(\ldots 6s6d\ ^1D_2)$, corresponding to features 6 (figure 1) and 8 (figure 2) respectively, dominant LS terms indicate strongly dipole-allowed excitations. These two excitations are among the strongest of those measured. The UDWA calculations show good agreement with the measured DCS for feature 8 although CCC theory provides a closer match to the data.

Another strong excitation is that associated with feature 1 (figure 3) for the blended final level X = $(\ldots 5d^2\ ^1D_2 + \ldots 6p5d\ ^1D_2)$ comprising even- and odd-parity $^1D_2$ terms

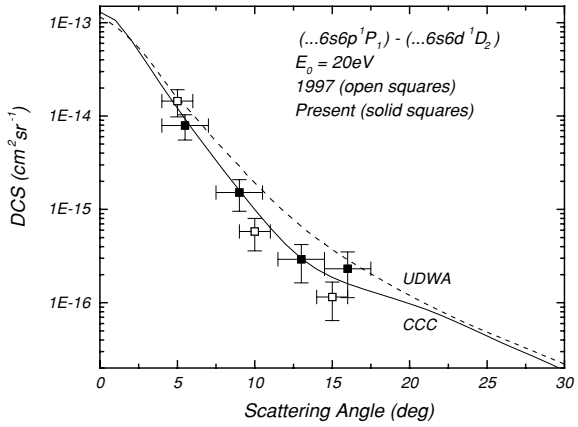

Figure 2. Differential cross sections for the (. . . 6s6p $^1P_1$) to (. . . 6s6d $^1D_2$) excitation at 20 eV. Solid squares with error bars represent the results measured in the present work. The solid curve shows the results of a CCC calculation [3]. Open squares with error bars represent the measured PDCS of Zetner *et al* [5] converted to DCS by the procedure outlined in the text. The dashed curve is a UDWA calculation of the DCS as described in [5].

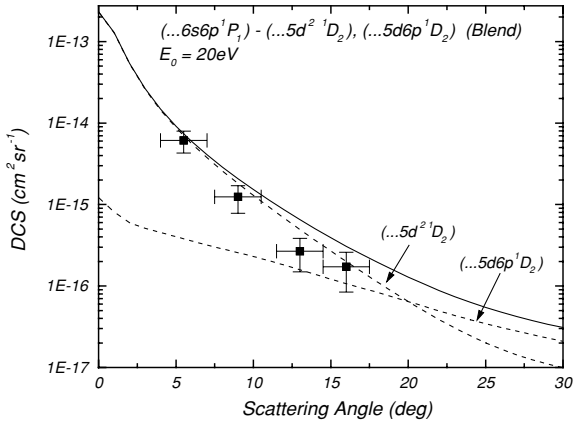

Figure 3. Differential cross sections for the (. . . 6s6p $^1P_1$) to blended (. . . 5d^2 $^1D_2$ + . . . 5d6p $^1D_2$) excitation. Dashed curves show CCC results for the resolved excitation in the blend.

(predominantly). Calculations show the small angle DCS of the blended feature to be determined largely by the even parity (. . . 5d^2 $^1D_2$) component. Inspection of table 1 of Johnson *et al* [3] reveals many dipole-allowed (single-electron) transitions of the types 6p → 6d, 5d → 6p made possible by a substantial (. . . 6p5d ^1P) term in the expansion of the (. . . 6s6p $^1P_1$) initial state wavefunction. Excitation of the odd-parity (. . . 6p5d $^1D_2$) component of the blend is completely dipole forbidden and very weak in forward scattering.

The DCS for feature 3 (figure 4) is weaker than those already discussed. The final level here is X = (5d^2 $^3P_2$). Although, nominally a ^3P level, the CI expansion shows significant admixture of ^1D terms. Apparently, dipole-allowed excitations of the 6p → 6d and 5d → 6p types, originating on the (. . . 6p5d ^1P) component of the initial ^1P level, produce the forward-peaking nature of this transition. For this transition, the UDWA results do not show good agreement with the data.

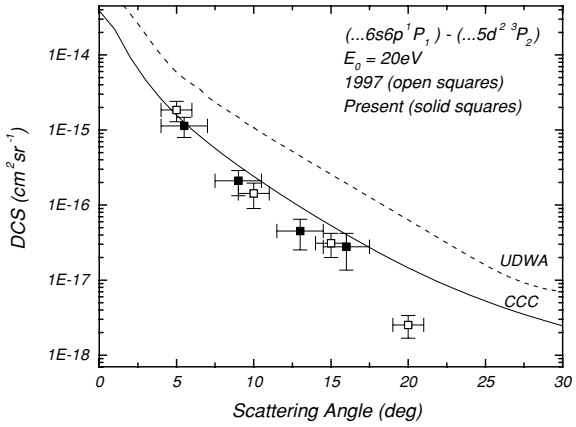

Figure 4. Same as figure 2 except for the (. . . 6s6p ^{1}P$_1$) to (. . . 5d^2 ^{3}P$_2$) excitation.

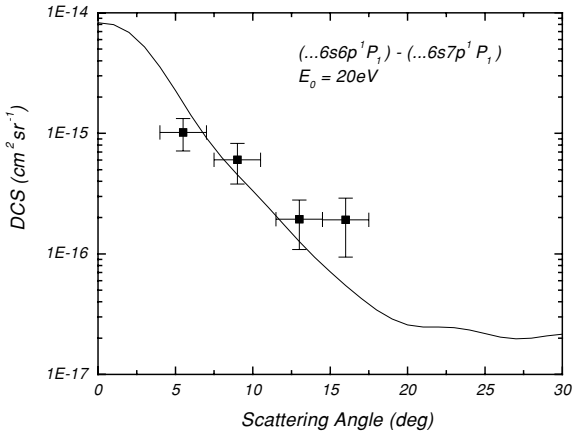

Figure 5. Same as figure 1 except for the (. . . 6s6p ^{1}P$_1$) to (. . . 6s7p ^{1}P$_1$) excitation.

Finally, the weakest transition studied, feature 7 (figure 5), terminates on the X = (. . . 6s7p ^{1}P$_1$) level. This is a dipole-forbidden excitation by virtue of the odd parity of both final and initial levels. However, both initial and final levels contain (. . . 6s7p ^{1}P$_1$) terms in the CI expansion. This indicates an elastic scattering component to the transition which may explain the forward peaking of the DCS.

Conclusions

We have measured electron impact DCS for several excitations of the type (. . . 6s6p ^{1}P$_1$) $\rightarrow$ X at 20 eV impact energy. Recently published EICP were utilized to account for the anisotropic magnetic sublevel populations produced by laser excitation of the (. . . 6s6p ^{1}P$_1$) level. All the DCS show forward-peaking behaviour consistent with dipole allowed and elastic contributions to the excitation. The measured DCS are well described by CCC theory. Available UDWA calculations show good agreement in the case of a strong, dipole-allowed transition (feature 8) but are unable to reproduce the data for the weaker feature 3, terminating on a ^{3}P$_2$ level.

Acknowledgments

The authors gratefully acknowledge funding for this work by the Natural Sciences and Engineering Research Council of Canada. They would also like to thank D Fursa and G Csanak for enlightening discussion and for providing the CCC and UDWA calculations, respectively, used in this work.

References

[1] Fursa D V, Trajmar S, Bray I, Kanik I, Csanak G, Clark R E H and Abdallah J Jr 1999 *Phys. Rev.* A **60** 4590–9
[2] Fursa D V, Bray I, Csanak G, Clark R E H, Abdallah J Jr, Kanik I and Trajmar S 2002 *Phys. Rev.* A **65** 032723
[3] Johnson P V, Zetner P W, Fursa D and Bray I 2002 *Phys. Rev.* A **66** 022707
[4] Johnson P V and Zetner P W 2005 *J. Phys. B: At. Mol. Opt. Phys.* **38** 2793–810
[5] Zetner P W, Trajmar S, Wang S, Kanik I, Csanak G, Clark R E H, Abdallah J Jr and Nickel J C 1997 *J. Phys. B: At. Mol. Opt. Phys.* **30** 5317–39
[6] Johnson P V, Eves B, Zetner P W, Fursa D and Bray I 1999 *Phys. Rev.* A **59** 439–54
[7] Li Y and Zetner P W 1996 *J. Phys. B: At. Mol. Opt. Phys.* **29** 1803–16
[8] Wang S, Trajmar S and Zetner P W 1994 *J. Phys. B: At. Mol. Opt. Phys.* **27** 1613–21